# Confining the spin between two metal atoms within the carbon cage: Redox-active metal-metal bonds in dimetallofullerenes and their stable cation radicals

Nataliya A. Samoylova,[a] Stanislav M. Avdoshenko,[a] Denis S. Krylov,[a] Hannah R. Thompson,[b] Amelia C. Kirkhorn,[b] Marco Rosenkranz,[a] Sandra Schiemenz,[a] Frank Ziegs,[a] Anja U. B. Wolter,[a] Shangfeng Yang,[c] Steven Stevenson,*[b] Alexey A. Popov*[a]

## Supporting Information

## Experimental details

**Synthesis of $Er_2S@C_{82}$.** Two graphite rods of 10 cm length and 6 mm diameter were drilled and filled with a mixture of metal, graphite powder, and guanidium thiocyanate in a molar ratio of 1:12.5:2.5. Then, the rods were mounted inside the fullerene generator on two electrodes, which were linked to an electric arc generator. The walls of the chamber and the electrodes were water-cooled throughout the synthesis process. Before burning, the chamber was filled with Helium again at a pressure of 200 mbar. According to the previous work, the current was set in the form of square signal with 100A at the high point. Two rods were evaporated alternatively and there was a breaking between two impulses to let the generator cool down and stabilize.

**HPLC separation.** Fullerene separation was achieved by multistage high performance liquid chromatography (HPLC) with pure toluene as the eluent. In the first stage, the soot extract was separated into several fractions using linear combination of two analytical 4.6 x 250 mm Buckyprep columns (Nacalai Tesque) with a flow rate of 1.6 mL/min and an injection volume of 800 µL. Some subfractions were then further separated or isolated by recycling HPLC with a semi-preparative 10 x 250 mm Buckyprep or Buckyprep-M columns (Nacalai Tesque) with a flow rate of 1-3 mL/min and an injection volume of 5 mL.

**Spectroscopic and physicochemical measurements. MALDI mass-spectra** were measured with a Bruker autoflex mass-spectrometer. ***UV-vis-NIR absorption spectra*** were measured in toluene solution at room temperature with Shimadzu 3100 spectrophotometer. ***Raman spectra*** were recorded at 78 K on a T 64000 triple spectrometer (Jobin Yvon) using a 647 nm excitation wavelength of the Kr laser. For Raman measurements, the samples were drop-coated onto single-crystal KBr disks. ***IR spectra*** were measured on KBr substrates using Vertex 80 FT-IR spectrometer (Bruker, Germany). The 125 MHz $^{13}C$ ***NMR spectra*** were measured at room temperature with $d^6$-acetone as a lock on an Avance 500 spectrometer (Bruker, Germany) using the multiprobe head PH 1152Z. ***Voltammetric experiments*** were performed in *o*-dichlorobenzene solution with $TBABF_4$ electrolyte salt in a glove box using potentiostat-galvanostat PARSTAT 4000A. A three-electrode system using a platinum working and a counter electrode and a silver wire reference electrode was used. Potentials were measured by adding ferrocene as an internal standard. X-band ***EPR spectra*** were measured at room temperature using a Bruker EMXmicro spectrometer. ***Magnetization measurements*** were performed using a Quantum Design VSM MPMS3 magnetometer. The samples were drop-casted from either toluene ($Er_2@C_{82}$-$C_{3v}$, $Er_2S@C_{82}$-$C_{3v}$) or from o-dichlorobenzene ($[Er_2@C_{82}\text{-}C_{3v}]^+SbCl_6^-$) into standard polypropylene capsules. Magnetization curves of the fresh sample and the one measured several months after the sample preparation were virtually identical indicating the reasonable stability of the salt (the sample was kept in the glovebox but had inevitable contact to air prior to the SQUID measurements).

**Computational studies.** DFT optimization of molecular structures were first performed using PBE functional and original basis set of TZ2P quality implemented in Priroda code.[1, 2] Molecular dynamics simulations were performed at the PBE/DZVP using CP2K code.[3, 4] Calculations employed Nose-Hover thermostat set at 300 K. Additional calculations of spin density and *hfc* coupling constants were performed with the Orca suite at the PBE level with TZVP basis set for carbon atoms and def2-TZVP basis set for Sc.[5] The magnetic susceptibility tensor was computed using PHI code,[6] which employed crystal-field parameters obtained *ab initio* at the CASSCF/SO-RASSI level using the SINGLE_ANISO module[7] implemented in MOLCAS 8.0.[8]

## References

1. D. N. Laikov and Y. A. Ustynuk, *Russ. Chem. Bull.*, 2005, **54**, 820-826.
2. J. P. Perdew, K. Burke and M. Ernzerhof, *Phys. Rev. Lett.*, 1996, **77**, 3865-3868.
3. J. VandeVondele, M. Krack, F. Mohamed, M. Parrinello, T. Chassaing and J. Hutter, *Comput. Phys. Commun.*, 2005, **167**, 103-128.
4. J. Hutter, M. Iannuzzi, F. Schiffmann and J. VandeVondele, *WIREs Comput. Mol. Sci.*, 2014, **4**, 15-25.
5. F. Neese, *WIREs Comput. Mol. Sci.*, 2012, **2**, 73-78.
6. N. F. Chilton, R. P. Anderson, L. D. Turner, A. Soncini and K. S. Murray, *J. Comput. Chem.*, 2013, **34**, 1164-1175.
7. L. F. Chibotaru and L. Ungur, *J. Chem. Phys.*, 2012, **137**, 064112.
8. F. Aquilante, J. Autschbach, R. K. Carlson, L. F. Chibotaru, M. G. Delcey, L. De Vico, I. Fdez. Galván, N. Ferré, L. M. Frutos, L. Gagliardi, M. Garavelli, A. Giussani, C. E. Hoyer, G. Li Manni, H. Lischka, D. Ma, P. Å. Malmqvist, T. Müller, A. Nenov, M. Olivucci, T. B. Pedersen, D. Peng, F. Plasser, B. Pritchard, M. Reiher, I. Rivalta, I. Schapiro, J. Segarra-Martí, M. Stenrup, D. G. Truhlar, L. Ungur, A. Valentini, S. Vancoillie, V. Veryazov, V. P. Vysotskiy, O. Weingart, F. Zapata and R. Lindh, *J. Comput. Chem.*, 2016, **37**, 506-541.

## Separation of Er-EMFs

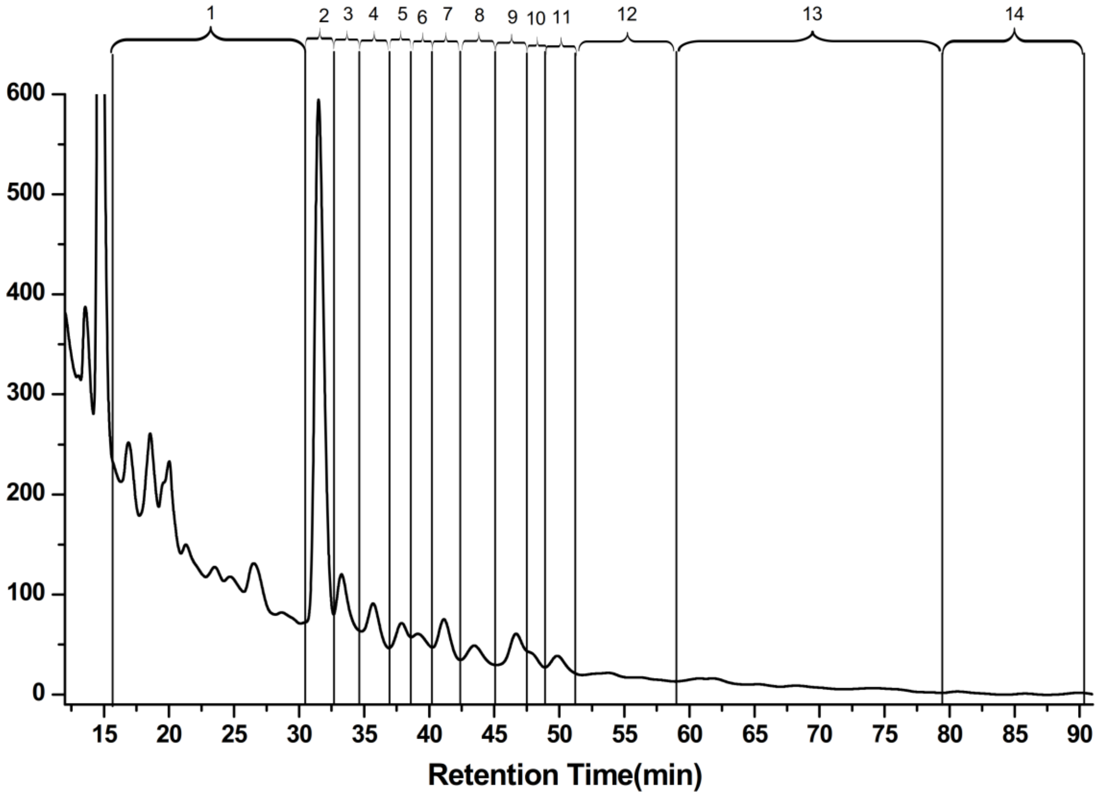

**Figure S1.** Stage 1 HPLC separation chromatogram of erbium-containing system on a Buckyprep column: HPLC profile of the raw fullerene extract and numbers of the collected fractions

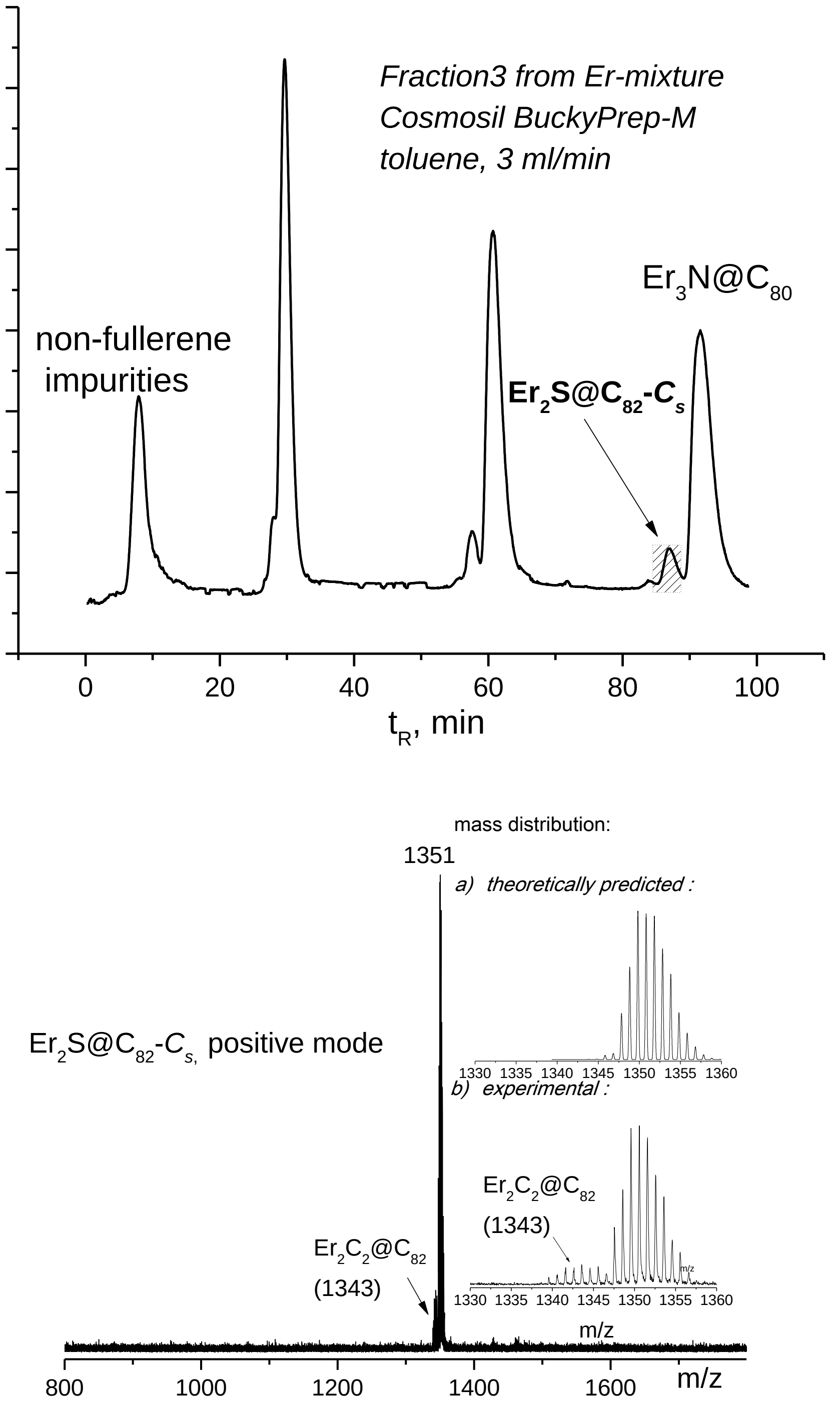

**Figure S2.** Recycling HPLC separation and mass-spectrum of $Er_2S@C_{82}$-$C_s$(6)

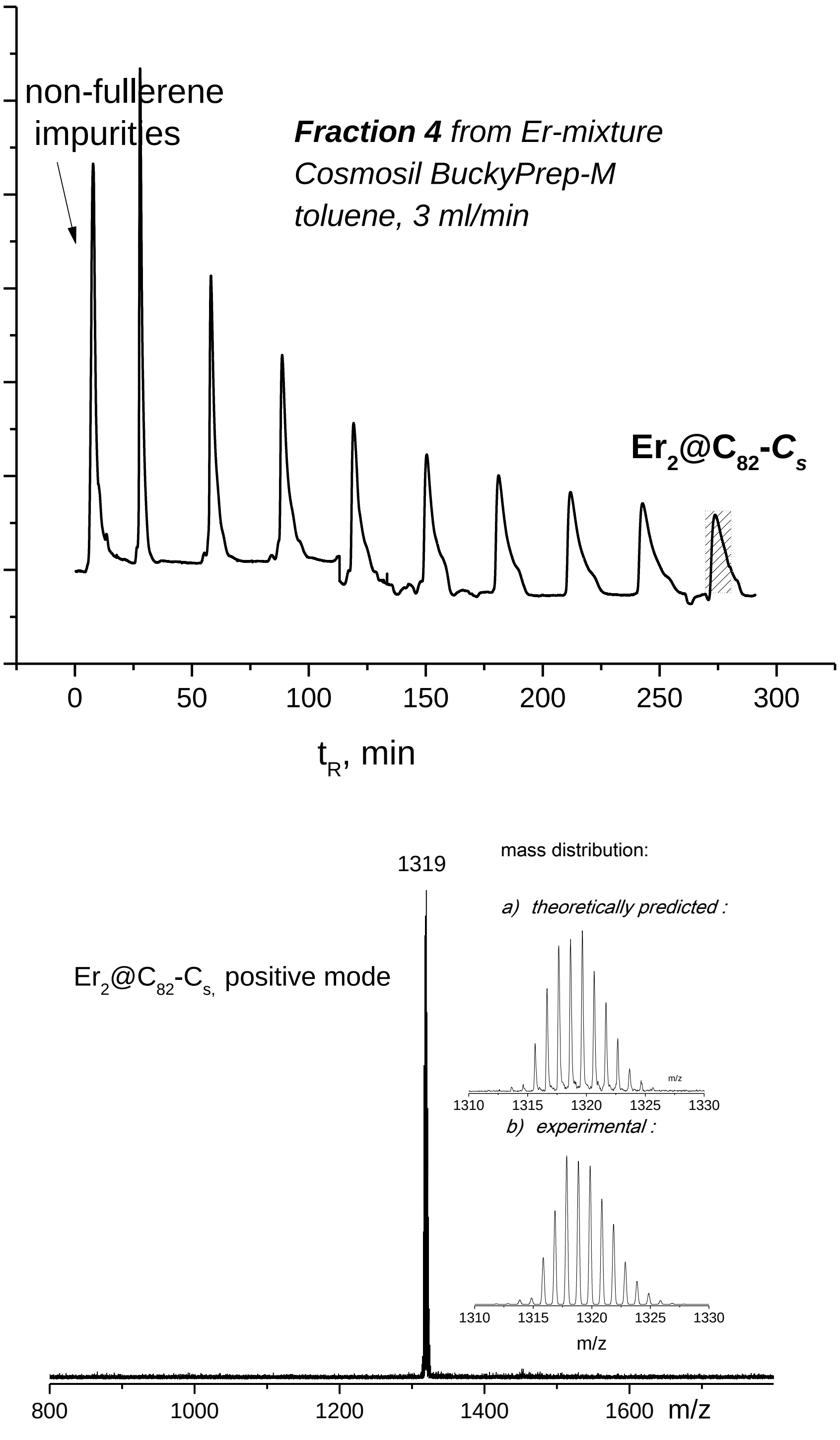

**Figure S3.** Recycling HPLC separation and mass-spectrum of $Er_2@C_{82}$-$C_s$(6)

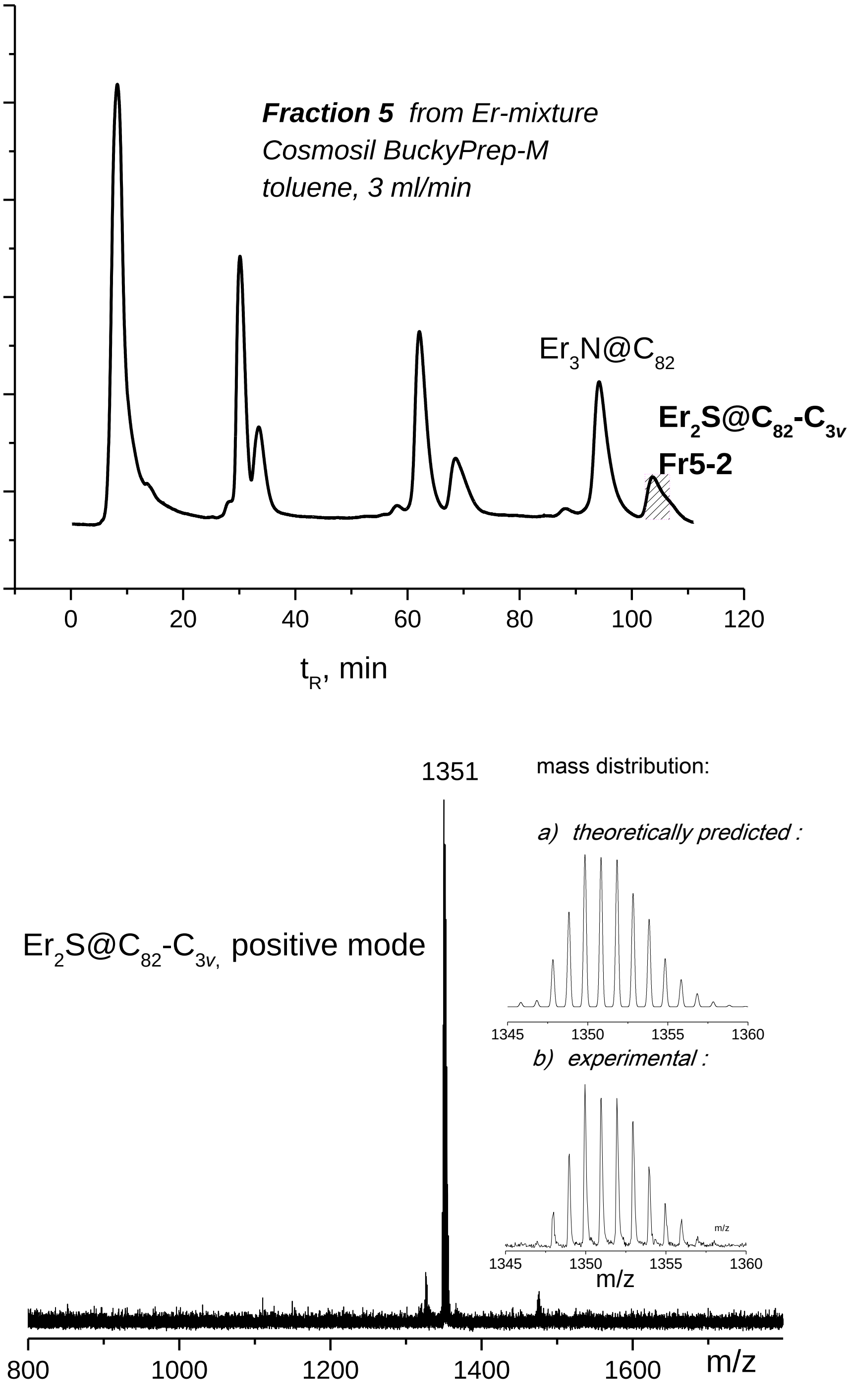

**Figure S4.** Recycling HPLC separation and mass-spectrum of $Er_2S@C_{82}$-$C_{3v}$(8)

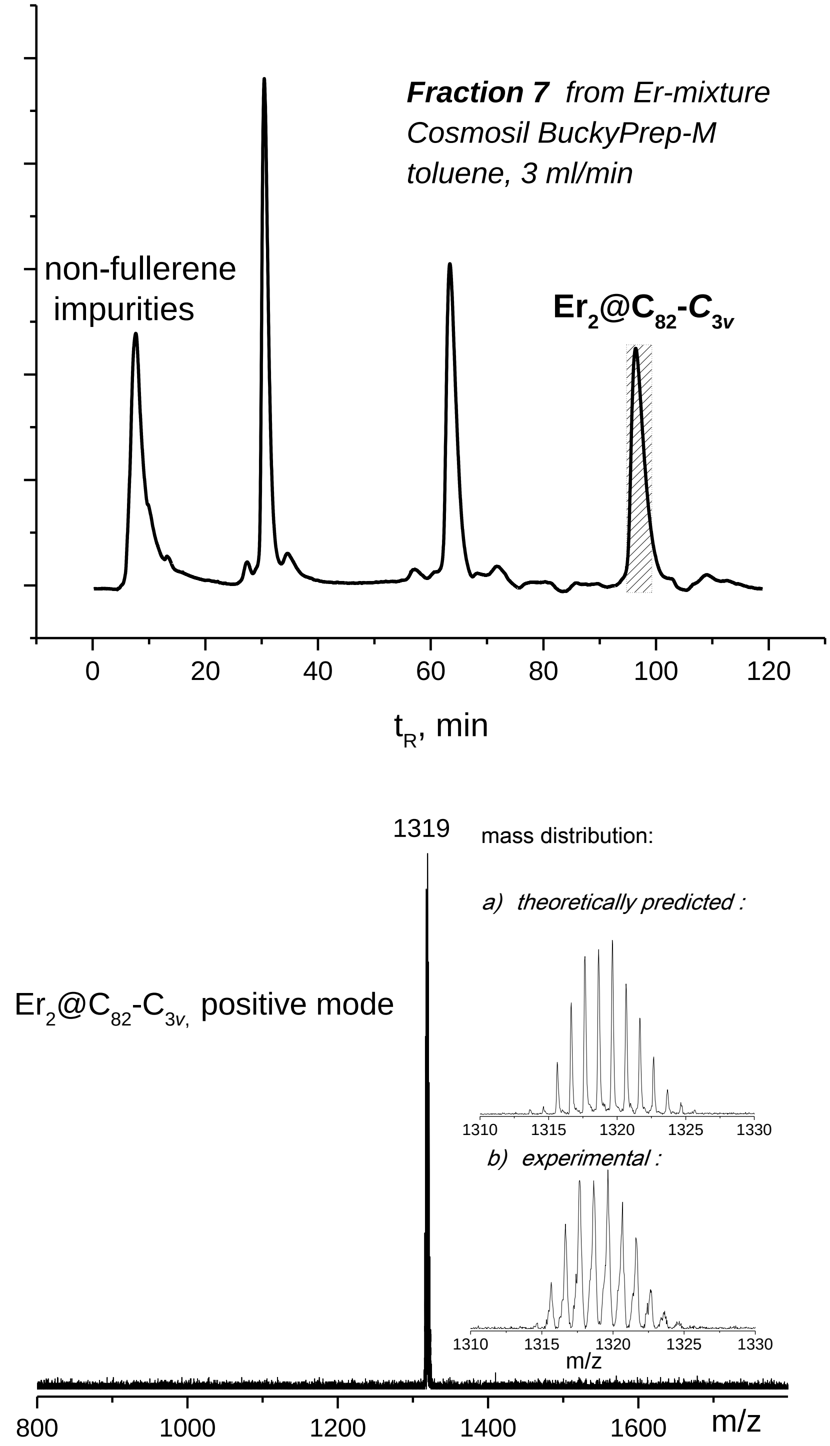

**Figure S5.** Recycling HPLC separation and mass-spectrum of $Er_2S@C_{82}$-$C_{3v}$(8)

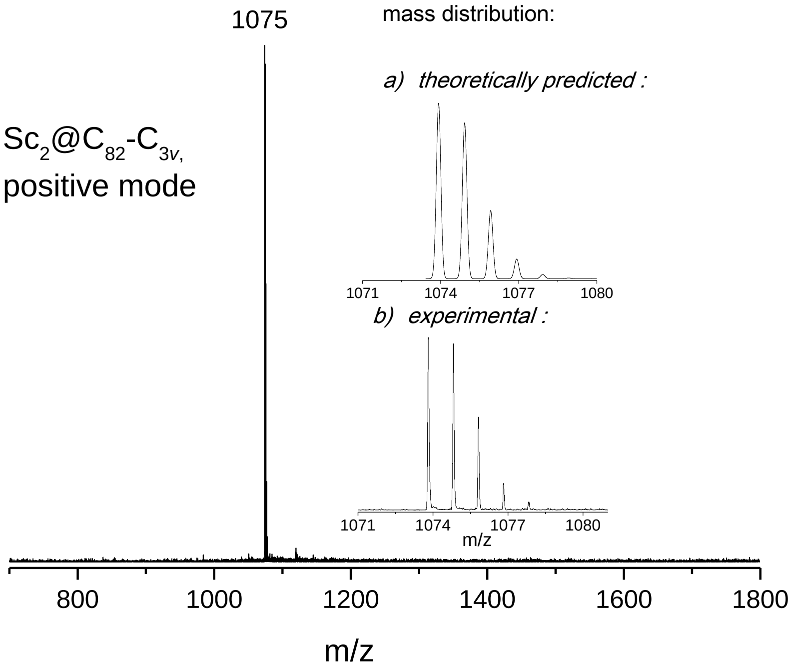

**Figure S6.** Mass-spectrum of Sc$_2$@C$_{82}$-$C_{3v}$(8)

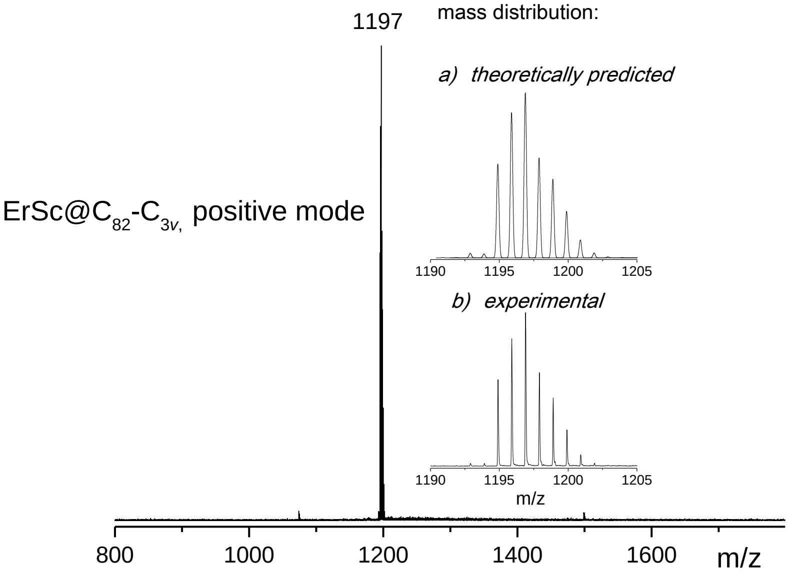

**Figure S7.** Mass-spectrum of ErSc@C$_{82}$-$C_{3v}$(8)

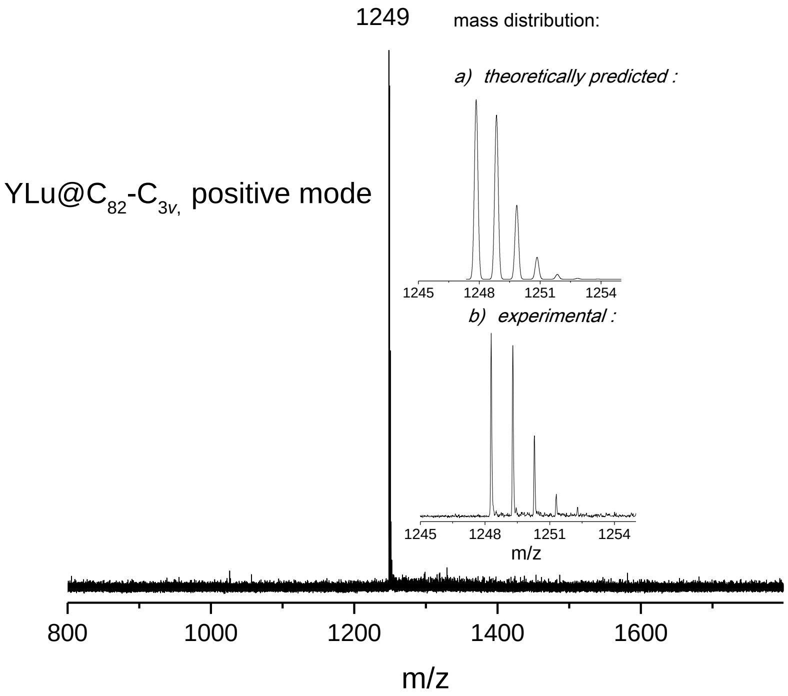

**Figure S8.** Mass-spectrum of YLu@$C_{82}$-$C_{3v}$(8)

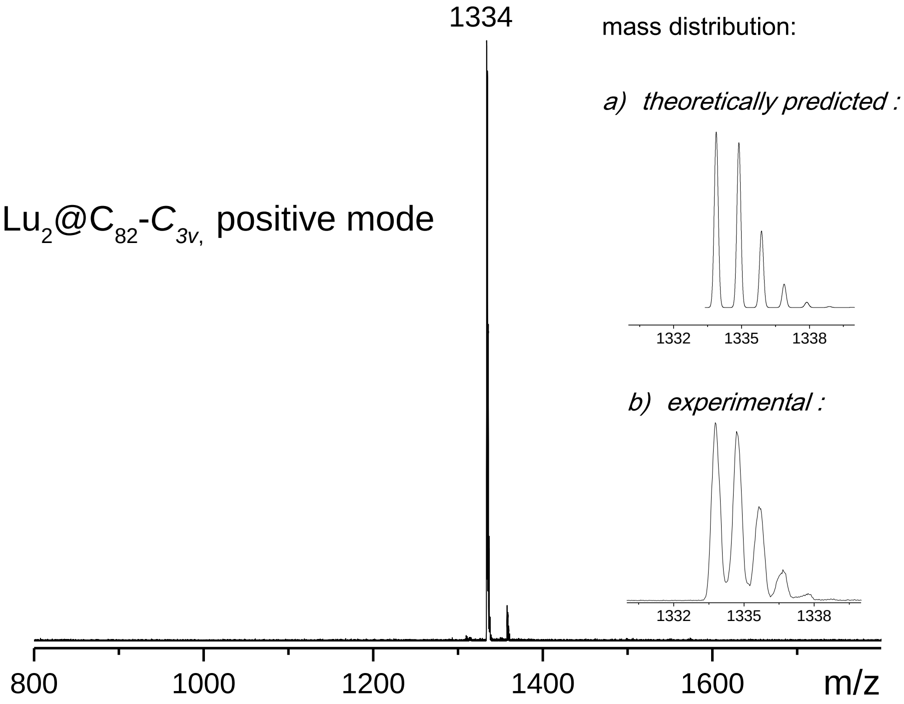

**Figure S9.** Mass-spectrum of Lu$_2$@C$_{82}$-$C_{3v}$(8)

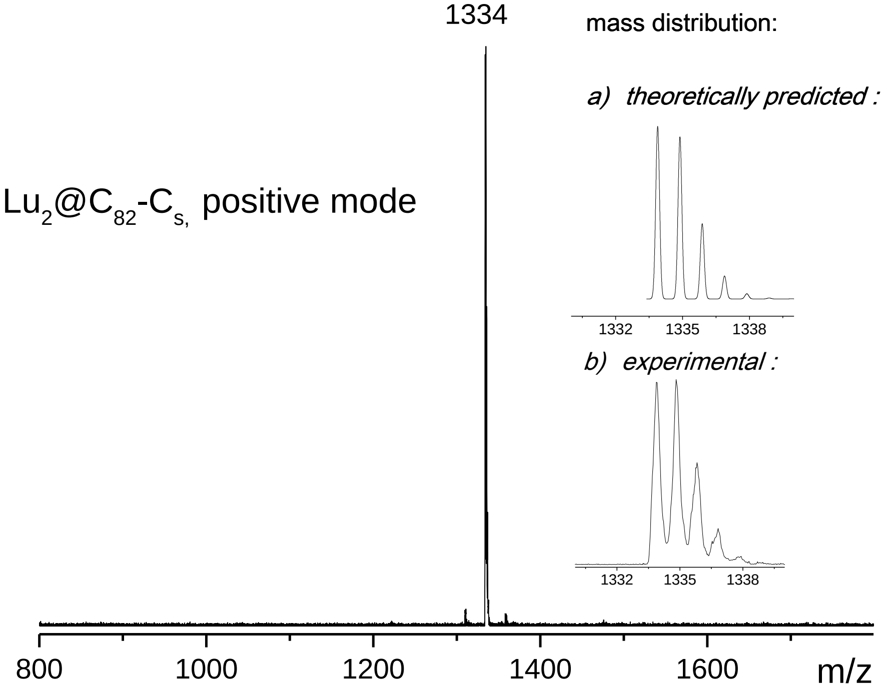

**Figure S10.** Mass-spectrum of Lu$_2$@C$_{82}$-$C_s$(6)

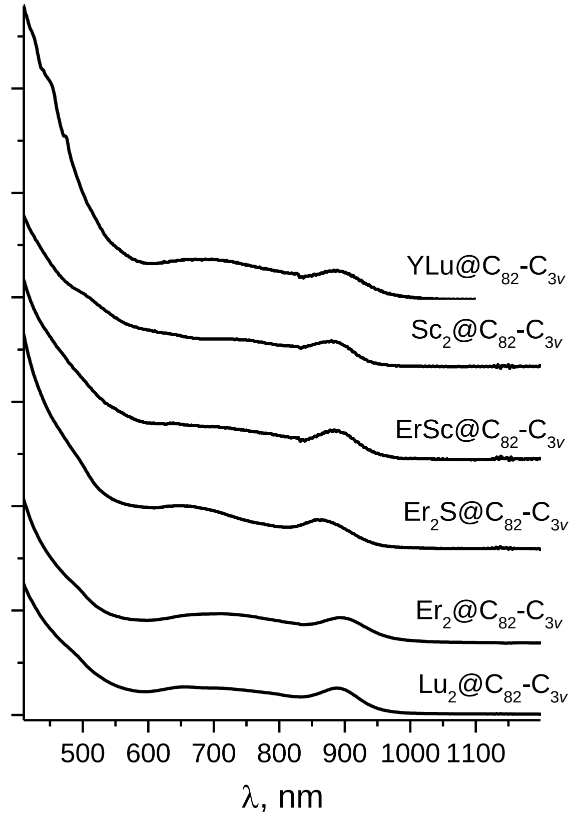

**Figure S11.** Absorption spectra of $M_2@C_{82}$-$C_{3v}$(8) dimetallofullerenes in toluene solution

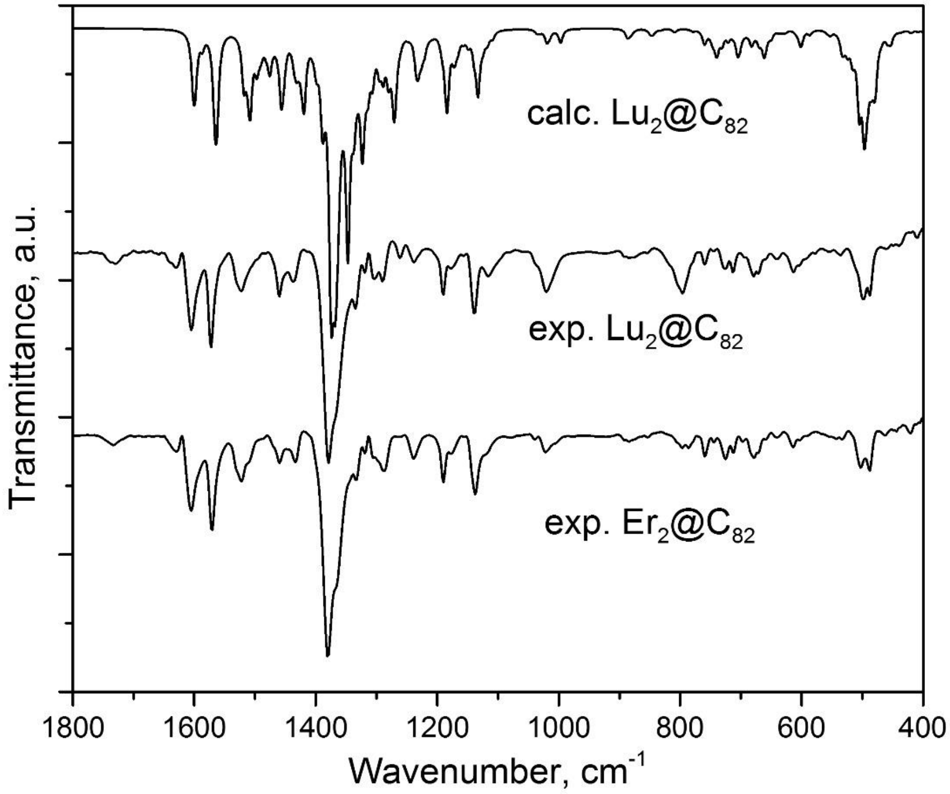

**Figure S12.** Experimental IR spectra of $Er_2@C_{82}$-$C_{3v}$ and $Lu_2@C_{82}$-$C_{3v}$ compared to the computed spectrum for $Lu_2@C_{82}$-$C_{3v}$.

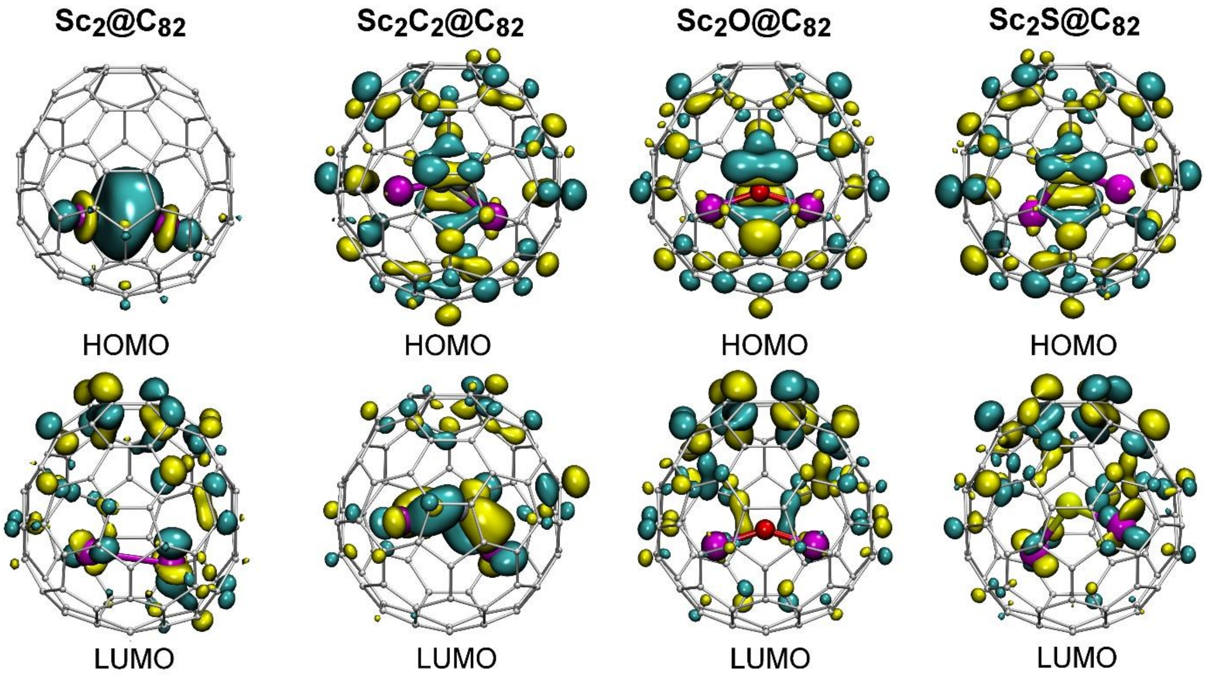

**Figure S13.** Frontier molecular orbitals of $Sc_2@C_{82}$, $Sc_2C_2@C_{82}$, $Sc_2O@C_{82}$, and $Sc_2S@C_{82}$, all with $C_{3v}(8)$ fullerene cage, computed at the PBE/TZVP level

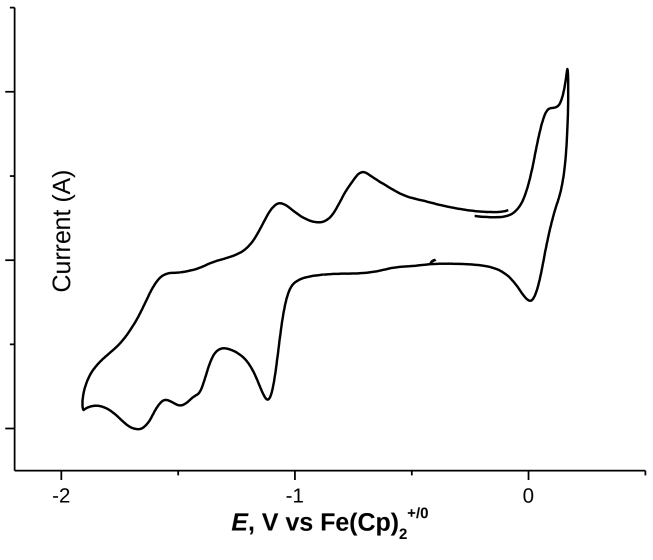

**Figure S14.** Cyclic voltammogram of $Sc_2@C_{82}$-$C_{3v}$

## Line width analysis in the EPR spectrum of $Sc_2@C_{82}^+$

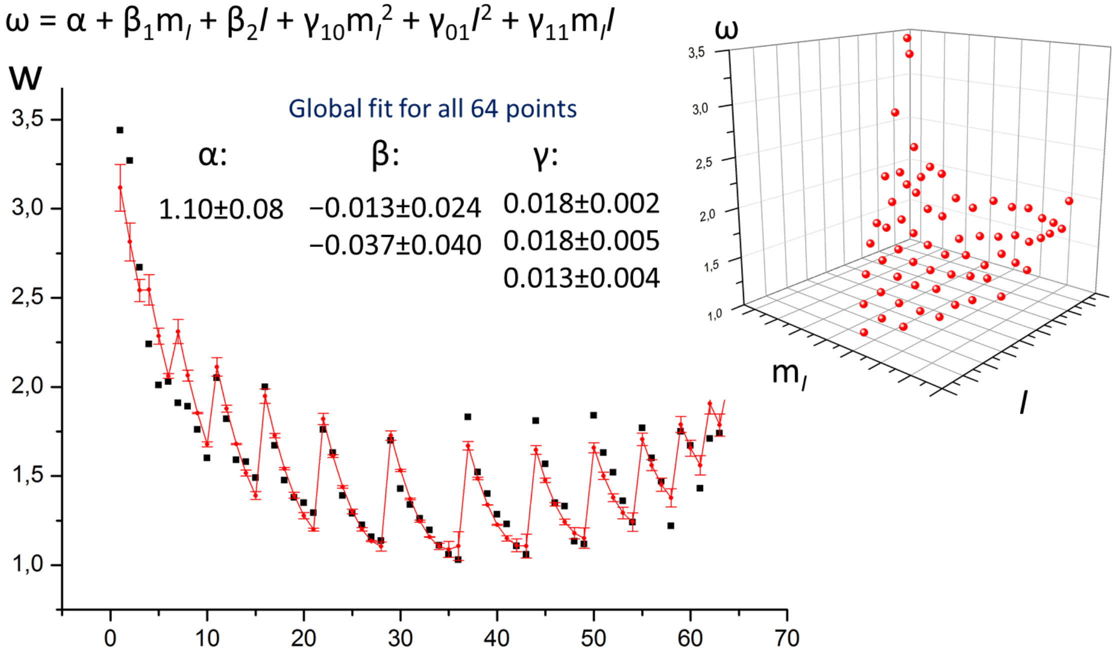

**Figure S15.** Linewidth in the EPR spectrum of $Sc_2@C_{82}^+$ as a function if $I$ and $m_I$ and the fit of the whole set of data using quadratic function of both parameters

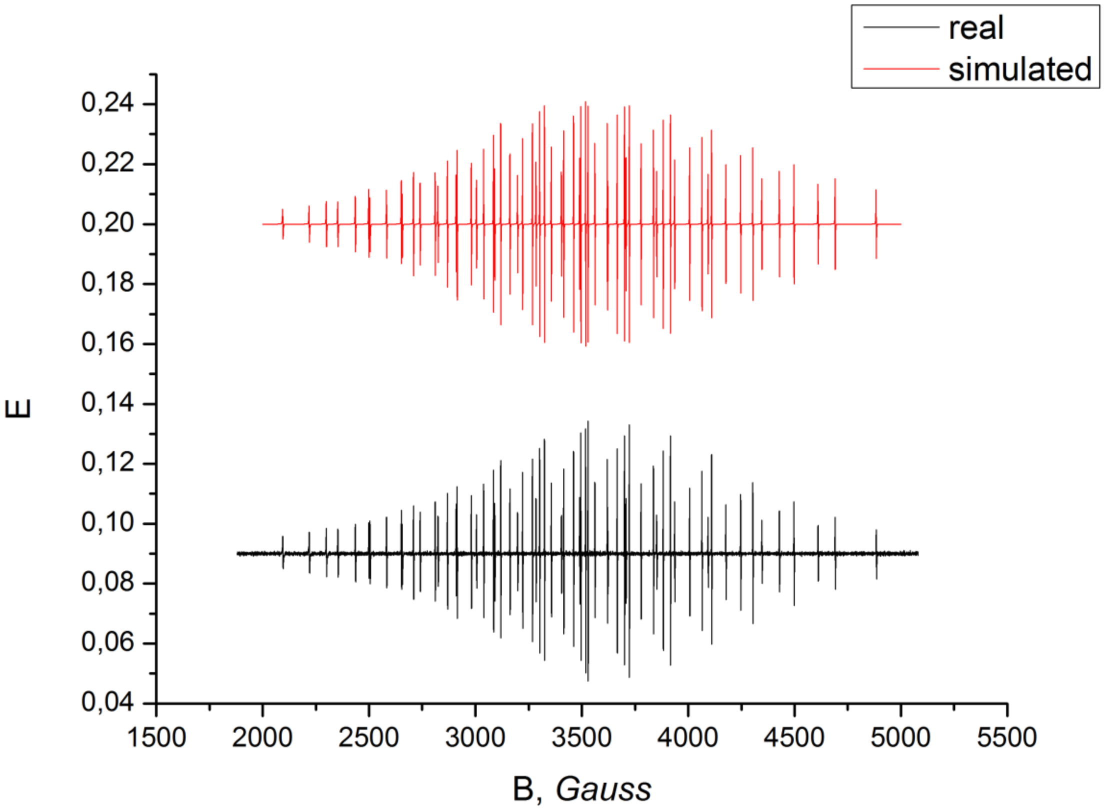

**Figure S16.** Comparison of experimental (black) and simulated (red) EPR spectra of $Sc_2@C_{82}^+$. For the sake of comparison, noise reduction was applied to the experimental spectrum by filtering high-frequency part in the Furrier-transformed spectrum. Original experimental spectrum is shown in Fig. 10 in the main manuscript. Positions of the lines in simulated spectrum were obtained using XSophe software, linewidth are from the fit described in Fig. S15.

## Ab initio calculations of magnetic properties

Ab initio energies and wave functions of CF multiplets for the $Er_2S@C_{82}$, $Er_2@C_{82}$ molecules have been calculated using the quantum chemistry package MOLCAS 8.0. Each Er(III) atom in the system was considered independently, while the second metal in the system was f-electron free (Yttrium). Single point complete active space self-consistent field with spin-orbit interactions calculations (CASSCF/SO-RASSI) level of theory was employed to derive ab initio values (**Tables S1-S3**). Assuming $^4I_{15/2}$ ground state multiplet, which results in eight low-lying Kramers doublets. The active space of the CASSCF calculations includes eleven active electrons and the seven active orbitals (e.g. CAS (11,7)). All 35 quartet states and 112 doublets were included in the state-averaged CASSCF procedure and were further mixed by spin-orbit coupling in the RASSI procedure. Atomic natural extended relativistic basis set (ANO-RCC) was employed with VDZ-quality of Y, Er. The single ion magnetic properties and CF-parameters were calculated with use of SINGLE_ANISO module, and then used for the analysis with the PHI code.

**Table S1.** *CASSCF/SO-RASSI/SINGLE_ANISO + PHI calculations results summary for the* $Er_2@C_{82}$*-*$C_{3v}$ *molecule. G-tensors components and energies of the eight low lying KD of the Er1 and Er2 ions.*

| Kramers Doublet | **Er1** | | **Er2** | |
|---|---|---|---|---|
| KD# | state energy, $cm^{-1}$ | $g_x$ \| $g_y$ \|$g_z$, μb | state energy, $cm^{-1}$ | $g_x$ \| $g_y$ \|$g_z$, μb |
| KD1 | 0.0 | 10.18\|7.87\|0.43 | 0.0 | 10.18\|7.87\|0.43 |
| KD2 | 55.9 | 6.22\|4.52\|0.89 | 55.9 | 6.22\|4.52\|0.89 |
| KD3 | 162.6 | 0.58\|1.22\|11.81 | 162.6 | 0.58\|1.22\|11.81 |
| KD4 | 207.4 | 1.10\|2.18\|8.99 | 207.4 | 1.10\|2.18\|8.99 |
| KD5 | 249.1 | 0.44\|3.76\|7.46 | 249.1 | 0.44\|3.76\|7.46 |
| KD6 | 284.7 | 5.24\|3.83\|0.70 | 284.7 | 5.24\|3.83\|0.70 |
| KD7 | 378.4 | 1.28\|1.82\|6.96 | 378.4 | 1.28\|1.82\|6.96 |
| KD8 | 554.5 | 0.04\|0.06\|7.09 | 554.5 | 0.04\|0.06\|7.09 |

**Table S2.** *CASSCF/SO-RASSI/SINGLE_ANISO + PHI calculations results summary for the* $Er_2S@C_{82}$*-*$C_{3v}$ *molecule. G-tensors components and energies of the eight low lying KD of the Er1 and Er2 ions.*

| Kramers Doublet | **Er1** | | **Er2** | |
|---|---|---|---|---|
| KD# | state energy, $cm^{-1}$ | $g_x$ \| $g_y$ \|$g_z$, μb | state energy, $cm^{-1}$ | $g_x$ \| $g_y$ \|$g_z$, μb |
| KD1 | 0.0 | 1.66\|4.42\|14.71 | 0.0 | 1.81\|3.13\|15.38 |
| KD2 | 73.5 | 0.44\|3.61\|7.63 | 75.6 | 2.08\|4.79\|7.65 |
| KD3 | 106.6 | 3.43\|5.71\|7.97 | 109.3 | 0.37\|3.53\|14.57 |
| KD4 | 188.1 | 1.48\|6.17\|9.64 | 154.5 | 0.07\|1.37\|11.36 |
| KD5 | 230.4 | 2.03\|3.24\|10.09 | 213.9 | 2.69\|4.73\|7.23 |
| KD6 | 272.0 | 1.58\|2.60\|15.33 | 335.1 | 0.54\|1.64\|16.74 |
| KD7 | 370.1 | 0.68\|0.75\|15.54 | 346.7 | 2.12\|3.40\|13.57 |
| KD8 | 511.2 | 0.13\|0.18\|18.00 | 516.5 | 0.11\|0.13\|18.13 |

**Table S3.** *Ab-intio derived (SINGLE_ANISO) crystal field parameters in Stevens Notation B(q,k)(cm$^{-1}$)* of $Er_2S@C_{82}$, $Er_2@C_{82}$ *molecules*(all EMFs are with $C_{82}$-$C_{3v}$(8) cage).

| | | $Er_2@C_{82}$ | | $Er_2S@C_{82}$ | |
|---|---|---|---|---|---|
| **index** | | Er1 | Er2 | Er1 | Er2 |
| **k** | **q** | **B(q,k)** | **B(q,k)** | **B(q,k)** | **B(q,k)** |
| 2 | -2 | 3.47E-01 | 3.47E-01 | -3.01E-01 | 3.29E-01 |
| 2 | -1 | 2.42E-01 | -2.42E-01 | 4.15E-02 | 1.29E-01 |
| 2 | 0 | 2.21E+00 | 2.21E+00 | -1.02E+00 | -1.17E+00 |
| 2 | 1 | 4.53E-01 | -4.53E-01 | -2.06E+00 | -2.18E+00 |
| 2 | 2 | 1.61E-01 | 1.61E-01 | 2.58E+00 | 2.61E+00 |
| 4 | -4 | -1.29E-04 | -1.29E-04 | -8.73E-05 | 1.00E-03 |
| 4 | -3 | -3.40E-03 | 3.40E-03 | -2.19E-03 | 1.60E-03 |
| 4 | -2 | 6.06E-05 | 6.07E-05 | 1.68E-03 | -8.02E-05 |
| 4 | -1 | -1.88E-03 | 1.88E-03 | -5.97E-04 | -1.07E-05 |
| 4 | 0 | -3.70E-04 | -3.70E-04 | -3.56E-05 | 2.82E-04 |
| 4 | 1 | -1.41E-03 | 1.41E-03 | 2.40E-03 | -9.49E-04 |
| 4 | 2 | 1.52E-03 | 1.52E-03 | -1.59E-03 | -1.12E-03 |
| 4 | 3 | -4.22E-03 | 4.22E-03 | -1.88E-03 | -5.97E-03 |
| 4 | 4 | -2.00E-04 | -2.00E-04 | 7.66E-04 | 3.84E-03 |
| 6 | -6 | -1.53E-04 | -1.53E-04 | 1.98E-04 | -4.74E-04 |
| 6 | -5 | -1.92E-04 | 1.92E-04 | -2.03E-03 | -9.91E-04 |
| 6 | -4 | -4.63E-04 | -4.63E-04 | 2.25E-04 | -3.48E-04 |
| 6 | -3 | 9.05E-04 | -9.05E-04 | 1.27E-04 | -2.94E-04 |
| 6 | -2 | 9.00E-05 | 9.00E-05 | -4.35E-04 | -9.54E-06 |
| 6 | -1 | -5.81E-05 | 5.81E-05 | 9.39E-05 | 1.45E-04 |
| 6 | 0 | 4.54E-05 | 4.54E-05 | 3.03E-06 | -2.22E-05 |
| 6 | 1 | -2.54E-04 | 2.54E-04 | 2.48E-04 | 2.54E-04 |
| 6 | 2 | 1.68E-04 | 1.68E-04 | 3.71E-04 | 2.89E-04 |
| 6 | 3 | 4.07E-04 | -4.07E-04 | -5.76E-04 | -7.19E-04 |
| 6 | 4 | -9.74E-05 | -9.73E-05 | -1.35E-04 | -2.26E-04 |
| 6 | 5 | 2.09E-04 | -2.09E-04 | 4.04E-04 | 7.19E-04 |
| 6 | 6 | 8.14E-05 | 8.14E-05 | -1.16E-04 | -4.02E-04 |